Development and initial evaluation of a novel method for assessing tissue-specific plasma free fatty acid utilization in vivo using (R)-2-bromopalmitate tracer

Nicholas D. Oakes,[1,*] Ann Kjellstedt,[*] Gun-Britt Forsberg,[*] Tony Clementz,[*] Germán Camejo,[*] Stuart M. Furler,[†] Edward W. Kraegen,[†] Maria Ölwegård-Halvarsson,[*] Arthur B. Jenkins,[2,†] and Bengt Ljung[*]

Department of Pharmacology,* Astra-Hässle AB, S-431 83 Mölndal, Sweden, and the Garvan Institute of Medical Research,† Sydney, New South Wales, Australia

Abstract **We describe a method for assessing tissue-specific plasma free fatty acid (FFA) utilization in vivo using a non-β-oxidizable FFA analog, [9,10-^{3}H]-(R)-2-bromopalmitate (^{3}H-R-BrP). Ideally ^{3}H-R-BrP would be transported in plasma, taken up by tissues and activated by the enzyme acyl-CoA synthetase (ACS) like native FFA, but then ^{3}H-labeled metabolites would be trapped. In vitro we found that 2-bromopalmitate and palmitate compete equivalently for the same ligand binding sites on albumin and intestinal fatty acid binding protein, and activation by ACS was stereoselective for the R-isomer. In vivo, oxidative and non-oxidative FFA metabolism was assessed in anesthetized Wistar rats by infusing, over 4 min, a mixture of ^{3}H-R-BrP and [U-^{14}C] palmitate (^{14}C-palmitate). Indices of total FFA utilization (R^*_f) and incorporation into storage products (R_{fs}') were defined, based on tissue concentrations of ^{3}H and ^{14}C, respectively, 16 min after the start of tracer infusion. R^*_f, but not R_{fs}', was substantially increased in contracting (sciatic nerve stimulated) hindlimb muscles compared with contralateral non-contracting muscles. The contraction-induced increases in R^*_f were completely prevented by blockade of β-oxidation with etomoxir. These results verify that ^{3}H-R-BrP traces local total FFA utilization, including oxidative and non-oxidative metabolism. Separate estimates of the rates of loss of ^{3}H activity indicated effective ^{3}H metabolite retention in most tissues over a 16-min period, but appeared less effective in liver and heart. In conclusion, simultaneous use of ^{3}H-R-BrP and [^{14}C]palmitate tracers provides a new useful tool for in vivo studies of tissue-specific FFA transport, utilization and metabolic fate, especially in skeletal muscle and adipose tissue.**—Oakes, N. D., A. Kjellstedt, G-B. Forsberg, T. Clementz, G. Camejo, S. M. Furler, E. W. Kraegen, M. Ölwegård-Halvarsson, A. B. Jenkins, and B. Ljung. **Development and initial evaluation of a novel method for assessing tissue-specific plasma free fatty acid utilization in vivo using (R)-2-bromopalmitate tracer.** ***J. Lipid Res.*** **1999.** 40: **1155–1169.**

Supplementary key words metabolism • turnover • analog • muscle • liver • heart • adipose tissue • kinetics

Perturbations in lipid metabolism most likely play key roles in the pathogenesis of the metabolic disease states of obesity and non-insulin-dependent diabetes mellitus. Our understanding of lipid metabolism is currently limited, however, by an inadequate set of tools for evaluating lipid metabolism in vivo. While established techniques exist for assessing whole body lipid metabolism, using either calorimetry (1) or lipid tracer dilution studies (2), studies at the individual tissue level have been conducted mostly in vitro. Techniques for assessing in vivo metabolism in individual tissues have been traditionally limited to organs with accessible and dedicated venous drainage, using mass balance techniques (e.g., 3, 4). More general methods are required to quantify lipid utilization rates in key metabolic tissues such as liver, skeletal muscles, and fat. Such methods could then be used to complement and evaluate the functional significance of a growing body of tissue-specific data reporting treatment-induced alterations in the molecules involved in lipid metabolism (5–7).

Plasma long-chain free fatty acids (FFA) are transported in blood bound to albumin. Debate continues about their mechanism of entry into cells, whether by passive diffusion across the plasma membrane or facilitated transport via specific membrane-associated transporters (8). In the

Abbreviations: FFA, free fatty acid; EFA, esterified fatty acid; ^{3}H-R-BrP, [9,10-^{3}H]-(R)-2-bromopalmitate; ^{14}C-P, [U-^{14}C]palmitic acid; ACS, acyl-CoA synthetase; R^*_f index of tissue-specific FFA utilization rate; R_{fs}', index of tissue-specific plasma FFA incorporation rate into storage; FABP, fatty acid binding protein; iFABP, intestinal FABP; CPT I, carnitine palmitoyl transferase I; DAUDA, 11-dansylamino undecanoic acid; HPLC, high performance liquid chromatography; WQ, white quadriceps; RQ, red quadriceps; WG, white gastrocnemius; RG, red gastrocnemius; EDL, extensor digitorum longus; WAT, white adipose tissue; BAT, brown adipose tissue; VLDL, very low density lipoprotein.

[1] To whom correspondence should be addressed.

[2] Present address: University of Wollongong, Wollongong, New South Wales, Australia.

Downloaded from www.jlr.org by guest, on June 14, 2012

cytosol FFAs are bound to fatty acid binding proteins (FABP). Metabolic sequestration is effected by acyl-CoA synthetase (ACS) which activates cytosolic FFA to the fatty acyl-CoA derivative. This activation is necessary for the major metabolic pathways of FFA metabolism, including β-oxidation and esterification, and therefore net flux through this reaction represents total fatty acid utilization. One principle for assessing tissue-specific FFA utilization is based on the use of a labeled fatty acid analog with a structural modification that does not interfere with cellular uptake and metabolic sequestration, but which alters subsequent metabolism to result in local trapping of the label. The partially metabolizable analog should not be a substrate for β-oxidation. Tissue accumulation of label would then be a function of total fatty acid utilization. An analogous principle has been applied successfully using radiolabeled 2-deoxyglucose to measure regional glucose metabolism (9). Several fatty acid analogs have been designed for the clinical assessment of myocardial metabolism (10–14). However these radiolabeled compounds are not readily available, utilize radioisotopes for external imaging, require specialist chemical facilities for synthesis, and have not been extensively evaluated for use in tissues other than myocardium.

Tracer-labeled 2-bromopalmitate is a potentially useful, partially metabolizable fatty acid analog for the assessment of tissue-specific fatty acid utilization. 2-Bromopalmitate binds to albumin and FABP (15) and indirect evidence suggests that it can be activated by ACS (16). It is not a substrate for β-oxidation in mitochondria or peroxisomes and has been used in pharmacological doses to inhibit fatty acid oxidation. This action is believed to be due to an effectively irreversible interaction of 2-bromopalmitoyl-CoA and carnitine palmitoyl transferase I (CPT I) which blocks transport of native long-chain fatty acyl CoAs into the mitochondria (17, 18). By the above reasoning, trapping at this metabolic site would ideally place 2-bromopalmitate tracer as an indicator of total FFA utilization. Finally, high specific activity ^{3}H- or ^{14}C-labeled 2-bromopalmitate can be produced using commercially available ^{3}H- or ^{14}C-labeled palmitate as starting material.

This report describes the theory, method, and initial experimental evaluation of a new technique for quantitative determination of tissue-specific FFA utilization in vivo based on the use of radiolabeled 2-bromopalmitate. In vitro studies were performed to verify that 2-bromopalmitate competes for the same transport protein ligand binding sites as native FFAs and that it is activated by the enzyme ACS. In vivo studies were conducted to assess the validity of the method, including the effectiveness of tissue trapping of radiolabeled products of 2-bromopalmitate tracer, and to obtain estimates of the ratio of radiolabeled 2-bromopalmitate to labeled palmitate activation rates in individual tissues. The results confirm that 2-bromopalmitate participates in FFA transport and reveal that activation by ACS is stereoselective for the R-enantiomer. Results of the in vivo studies demonstrate (R)-2-bromopalmitate tracer as a valuable tool for the assessment of tissue-specific total fatty acid utilization.

METHODS AND MATERIALS

2-Bromopalmitate binding to albumin and fatty acid binding protein

Fluorescence titration was used to compare binding of 2-bromopalmitate and palmitate to bovine serum albumin (BSA) and intestinal fatty acid binding protein (iFABP). The decrease in intrinsic fluorescence of BSA caused by the binding of fatty acids can be used to obtain average binding isotherms of this system (19, 20). Fatty acids and BSA were prepared in phosphate-buffered saline containing 2 mm calcium and magnesium. Relative affinities of palmitate and 2-bromopalmitate for BSA were established by titration of 1 μm solutions of initially fatty acid-free BSA with repeated additions of 2 μl of 1 mm solutions of the fatty acids. The BSA–fatty acid solution was held at 20°C and continuously stirred in a 2-ml cuvette. Readings were taken 4 min after each addition. Excitation and emission wavelengths were 290 nm and 370 nm, respectively. The respective slits were 2.5 and 4 nm and the integration time of the measurements after each addition of fatty acids was 2 s. The maximal quenching (Fmax/mol of bound fatty acid) was obtained in separate experiments in which fixed amounts of the fatty acids were titrated with an excess of BSA. Displacement of the fluorescent fatty acid probe 11-dansylamino undecanoic acid (DAUDA) from FABP by other ligands can be used to estimate relative affinities of these molecules for the protein (21). For the displacement experiments, 2-ml aliquots of 1 μm iFABP and 1 μm DAUDA were titrated with 2-μl consecutive additions of 50 μm palmitate or 2-bromopalmitate. All the solutions were made in phosphate-buffered saline. Reaction cells were maintained at 20°C and continuously stirred. Measurements were performed 4 min after additions. The decrease in emission at 500 nm was followed after excitation at 350 nm. Experiments were conducted in a LS-50B luminescence spectrometer (Perkin-Elmer, Norwalk, CT).

Activation of individual 2-bromopalmitate enantiomers by acyl CoA synthetase

Conversion of the individual R- and S-isomers of [9,10 ^{3}H]-2-bromopalmitate to their respective CoA esters by acyl CoA synthetase (ACS) was investigated using a hepatic microsomal preparation essentially as described in (22). Pieces of rat liver were homogenized in ten volumes of homogenization buffer (10 mm HEPES, pH 7.4, 1 mm EDTA, 5 mm DTT, 5 mm EGTA) using a Potter-Elvehjem homogenizer. The particulate fraction was cleared by centrifugation at 13000 *g* for 20 min at 4°C. The supernatant was then centrifuged at 140,000 *g* for 70 min at 4°C to pellet the microsomal fraction. The pellet was resuspended in homogenization buffer and stored in aliquots at −80°C. Reaction mixtures (50 μL) containing either [U-^{14}C]palmitic acid (^{14}C-P) or [9,10-^{3}H]-(R)-2-bromopalmitate (^{3}H-R-BrP) or [9,10-^{3}H]-(S)-2-bromopalmitate (^{3}H-S-BrP) together with 80–1500 μm palmitic acid, 1 mm coenzyme A, 10 mm ATP, 15 mm $MgCl_2$, 150 mm KCl, 5 mm DTT, 1.6 mm Triton X-100, and 100 mm Tris-HCl, pH 8.0, were preincubated for 3 min at 37°C. Reactions were initiated by the addition of microsomal material (10–100 $\mu g \cdot ml^{-1}$) and terminated after 5 min by spotting onto thin-layer chromatography plates (Silica Gel 60, AS Merck, Darmstadt). Plates were developed in chloroform–pyridine–formic acid–water 30:70:14:12. After drying, the plates were exposed on phosphoimager screens (Molecular Dynamics, Sunnyvale, CA) and detected spots were identified using standards and quantified.

Animal preparation

General. To briefly overview, studies were conducted in anesthetized rats, acutely prepared with jugular and carotid catheters. After a post-surgical stabilization period, radioactive tracers of

Downloaded from www.jlr.org by guest, on June 14, 2012

palmitate and 2-bromopalmitate were administered together as a constant 4-min infusion via a jugular catheter and frequent blood samples were collected from the carotid catheter for the determination of plasma tracer kinetics. The experiment was terminated with collection of tissue samples for analysis of tracer concentrations.

The experimental procedures were approved by the local ethics review committee on animal experiments (Göteborg region) and were in accordance with Swedish laws on the use and treatment of experimental animals. Adult male Wistar rats were maintained in a temperature-controlled (20–22°C) room with a 12 h light–dark cycle (lights on at 06:00) with free access to rodent chow (R3, Lactamin AB, Stockholm) and tap water. On the morning of the study, food was withdrawn at 07:00 and rats were anesthetized at 09:00 (Na-thiobutabarbitol 120 mg·kg^{-1}, Inactin®, RBI, Natick, MA). Body temperature was monitored using a rectal probe and maintained between 37°–38°C throughout the experiment. Animals were tracheotomized and catheters were placed in the right jugular vein and left carotid artery.

Unilateral hindlimb muscle contraction. Gluteal muscles were dissected to expose the left and right sciatic nerves. Both sciatic nerves were ligated and transected. The distal stump of the left sciatic nerve was pulled through custom-made silver ring electrodes for later stimulation. The rat was placed on its back and the left knee was flexed and fixed to a post with metal suture. The lower leg was held horizontal, with the foot in a flexed position, by attachment of the heel, using a suture under the Achilles tendon via a spring, to an adjustable beam. Some standardization of mechanical work of the lower leg muscles was provided by an in-line spring, stretched to a standard length using the beam adjustment. The ring electrode leads were connected to an electrical stimulator (Grass, SD9, Quincy, MA) via a stimulus isolator/current-supply (A385, World Precision Instruments, Sarasota, FL). Sciatic nerve stimulation (pulse frequency 1 Hz, pulse width 0.2 ms, supramaximal amplitude ~0.5 mA) was commenced 25 min before tracer infusion (1 h after completion of surgery and the hindlimb set-up procedure).

Experimental groups. Three groups of animals were studied (6 rats/group). Two groups were studied for estimating tissue specific FFA utilization rates: one group under control conditions and another group during fatty acid oxidation blockade with a carnitine palmitoyl transferase I inhibitor, etomoxir (RBI, Natick, MA). The etomoxir dose (20 μmol·kg^{-1}) was administered intravenously, in 200 μL sterile water, 20 min before tracer infusion. Tissues were collected from both of these groups 16 min after tracer infusion. In a third group of rats, studied to assess tissue trapping of tracer metabolites, tissues were removed 60 min after tracer administration, instead of 16 min.

Synthesis, resolution and identification of optical enantiomers of [9,10-^{3}H]-2-bromopalmitate

Racemic [9,10-^{3}H]-2-bromopalmitic acid was synthesized from [9,10-^{3}H]palmitic acid (1.96 TBq·mmol^{-1}, Amersham, Solna, Sweden) by a Hell-Volhard-Zelinsky reaction (23). Palmitic acid was treated with excess bromine and PCl_3 at 80°C overnight. The reaction was quenched with water and then bromine was removed by evaporation. Extraction with diethylether and purification by flash chromatography on silica gel using a gradient of 5–10% methanol and 0.2% acetic acid in chloroform yielded racemic [9,10-^{3}H]-2-bromopalmitic acid with a radiochemical purity of 99% according to thin-layer chromatography (chloroform–methanol–water–acetic acid in the volume proportions 65:25:3:0.1). The pure R- and S-enantiomers were obtained by chromatographic resolution on a Kromasil 100-CHI-TBB chiral column (EKA Chemicals, Bohus, Sweden) with 2.5% methyl-*t*-butylether and 0.1% acetic acid in hexane at 50°C (24). Radiochemical detection was used for collection. Assignment of absolute configurations of the separated R and S-enantiomers was accomplished by an enantioselective, lipase catalyzed, esterification of racemic [9,10-^{3}H]-2-bromopalmitic acid with n-butanol in hexane (25). After 65% conversion, the acid fraction was isolated and HPLC analysis showed only one peak coinciding with the slower eluting enantiomer from the chiral column. The optical rotation of this enantiomer was +22.8° (1% in $CHCl_3$, $[\alpha]^{25}_D$). The (+)-enantiomer has previously been assigned to have the R-configuration (26). The radiochemical purity of ^{3}H-labeled material used to prepare the infusate (described below) was >95% ^{3}H-R-BrP, as determined by HPLC.

Albumin–([9,10-^{3}H]-(R)-2-bromopalmitate)–([U-^{14}C] palmitate) complex for infusion

In vivo studies required the use of purified ^{3}H-R-BrP rather than the racemic mixture of R- and S-enantiomers (see below). Preliminary investigations revealed that extremely alkaline conditions cause racemization of purified ^{3}H-R-BrP. This precluded the use of methods based on the production of fatty acid soaps with hydroxide. The following procedure was therefore adopted. Infusates were prepared daily in quantities sufficient to perform experiments in two rats. Ethanol containing ~10^8 dpm ^{3}H-R-BrP, ~8×10^7 dpm ^{14}C-P (DuPont, Boston, MA) and 305 nmol Na-palmitate (Sigma, St. Louis, MO) was dried under a N_2 stream and reconstituted in 150 μl ethanol. The resulting solution was then added drop-wise to 0.6 ml of continuously stirred 4% (w:v) essentially FFA-free BSA (Sigma, St. Louis, MO) in normal saline. The infusate was made up to a final volume of ~2 ml by addition of normal saline.

Blood sampling and tracer infusion

All blood samples were collected via the carotid catheter. Catheter patency was maintained between samples by continuous infusion of a sterile saline solution containing Na_3-citrate (20.6 mm, 12 μl·min^{-1}). Immediately before tracer infusion, a 200-μl blood sample was collected for plasma free fatty acid (FFA), triglyceride, glucose, and insulin determinations (see below). The albumin–(^{3}H-R-BrP)–(^{14}C-P) complex was infused into the jugular vein at 230 μl·min^{-1} (Microinjection Pump, CMA/100, Carnegie Medicin, Stockholm, Sweden) for a total of 4 min. To obtain the plasma ^{3}H-R-BrP and ^{14}C-P activity time courses, blood samples (~170 μl) were collected from the carotid catheter 1, 2, 3, 4, 5, 6, 8, 12, and 16 min after the start of tracer infusion. Plasma was separated as quickly as possible by centrifugation and an aliquot (25 μl) was placed directly into 2 ml lipid extraction mixture (described below). Aliquots of the infusate were also collected into extraction mixture for later determination of total infusate activities.

Tissue sampling

After collection of the final blood sample, rats were killed with an overdose of thiobutabarbitol (120 mg·kg^{-1}). The following hindlimb muscles, from both legs, were collected: white quadriceps (WQ), red quadriceps (RQ), white gastrocnemius (WG), red gastrocnemius (RG), and extensor digitorum longus (EDL). In addition, white adipose tissue (WAT), from epididymal and inguinal depots, interscapular brown adipose tissue (BAT) as well as samples of diaphragm, heart, liver, kidney, stomach, and brain were collected. For measurement of total tissue ^{3}H and ^{14}C, freshly collected tissue pieces (~100 mg) were weighed and placed in small cardboard cones for combustion (see below). For investigation of ^{3}H metabolites of ^{3}H-R-BrP, in some experiments, tissues were rapidly dissected, frozen in liquid N_2-cooled tongs, and stored at −70°C awaiting analysis.

Analysis of plasma and tissue samples

Measurement of plasma substrates and insulin. Colorimetric kit methods were used for the measurement of plasma FFA (NEFA

Downloaded from www.jlr.org by guest, on June 14, 2012

C, Wako, Richmond, VA), triglyceride (Triglycerides/GB, Boehringer Mannheim, Indianapolis, IN), and glucose (Glucose HK, Roche, Stockholm, Sweden). Measurements were performed on a centrifugal analyzer (Cobas Bio, F. Hoffmann-La Roche & Co., Basle, Switzerland). Plasma insulin was determined using a rat insulin radioimmunoassay kit (Linco Research Inc., Charles, MO).

Resolution of plasma ^{3}H-R-BrP, ^3H_2O, and ^{14}C-P. In order to discriminate ^{3}H-R-BrP and ^{14}C-P from total ^{3}H and ^{14}C activities, a lipid extraction and separation procedure, based on the method of Hagenfeldt (27), was performed on plasma samples. Briefly, the method involved an initial acid lipid extraction, using a mixture of isopropanol–hexane–0.5 M H_2SO_4 40:10:1, followed by a polarity separation step, under alkaline conditions. This step partitions neutral lipids (including EFA) into a hexane phase and polar lipids (including FFA, e.g., ^{3}H-R-BrP and ^{14}C-P) into an alcohol phase. Small corrections were made for incomplete partitioning of ^{3}H-R-BrP and ^{14}C-P into the alcohol phase (see Appendix). ^3H_2O was estimated as the ^{3}H activity lost during evaporation of the lower isopropanol–water phase of the lipid extraction procedure.

Measurement of total plasma ^{3}H and ^{14}C levels. Total plasma and tissue ^{3}H and ^{14}C activities were determined using a Packard System 387 Automated Sample Preparation Unit (Packard Instrument Co., Inc., Meriden, CT) which completely oxidizes the sample and separates ^3H_2O and $^{14}CO_2$ into separate scintillation vials for counting. Sample ^{3}H and ^{14}C activities were measured using liquid scintillation spectrometry (Wallac 1409 counter; Wallac OY, Turku, Finland).

Analysis of plasma and tissue metabolites of [9,10-^{3}H]-(R)-2-bromopalmitate. Tissue (~200 mg) was homogenized in 2 ml of 2-propanol containing 0.1% acetic acid. To this was added 3 ml of hexane and 1 ml of saline buffer and the mixture was shaken at room temperature for 30 min. After centrifugation (1500 *g*, 5 min), the organic phase was evaporated under nitrogen and the residue was reconstituted in 100 μl of the mobile phase and injected onto the chiral column (described below). Plasma samples were prepared according to the procedure previously reported (24). After lipid extraction and phase separation, the aqueous phase was recovered and ^{3}H activity was measured in a liquid scintillation counter (Beckman 1409, Turku, Finland) with the scintillant Rialuma® (Lumac-LSC B.V., Groningen, The Netherlands). The chiral chromatographic column was a Kromasil-CHI-TBB, 250 × 4.6 mm I.D. (EKA Chemicals, Bohus, Sweden). The mobile phase consisted of hexane containing methyl-*t*-butyl ether (2.5%) and acetic acid (0.1%) as modifiers. The flow rate was 0.5 ml·min^{-1} and the column was thermostated at 50°C. An HPLC radioactivity monitor (Berthold LB 506 C-1, Bad Wildbad, Germany) was used for the detection of the labeled compounds.

Calculations

Index of tissue-specific plasma FFA utilization rate: calculation of R^*_f. We define the index of tissue-specific FFA utilization (R^*_f) as

$$R^*_f = \frac{C_P\, m_B}{\int_0^T c_B(t)\,dt} \qquad \text{Eq. 1)}$$

where C_P is the steady state arterial plasma FFA concentration, c_B is the arterial plasma concentration of ^{3}H-R-BrP as a function of time (t), produced by a short (4 min) infusion of ^{3}H-R-BrP, m_B is the tissue content of ^{3}H associated with metabolized products of ^{3}H-R-BrP (at $t = T$), and T is the time of tissue collection (=16 min). Derivation of this equation is described in the Appendix. Given the satisfaction of certain assumptions, R^*_f is in theory directly proportional to the true FFA utilization rate (R_f). We borrow the terminology of Sokoloff et al. (9) and refer to the constant of proportionality (LC^*) as the "lumped constant" i.e., ($LC^* = R^*_f / R_f$).

Whole body ^{3}H-R-BrP kinetics: calculation of plasma clearance rates. Plasma clearance rates of ^{3}H-R-BrP (CR_B) were estimated using the equation

$$CR_B = \frac{T_{in} i_B}{\int_0^\infty c_B(t)\,dt} \qquad \text{Eq. 2)}$$

where T_{in} is the exact tracer infusion time (4 min), i_B is the ^{3}H-R-BrP infusion rate and c_B is the plasma concentration of ^{3}H-R-BrP. A completely analogous expression was used for calculating clearance rates of ^{14}C-P.

Index of tissue-specific plasma FFA incorporation rate into storage: calculation of R_{fs}' and estimation of the lumped constant (LC^*). An estimate of the flux component of fatty acid utilization directed into storage (R_{fs}') was obtained from the expression

$$R_{fs}' = \frac{C_P m_P}{\int_0^T c_P(t)\,dt} \qquad \text{Eq. 3)}$$

where m_P is the tissue content of radioactivity associated with metabolized products of ^{14}C-P (at $t = T$), c_P is the arterial plasma ^{14}C-P concentration. The assumption here was that all ^{14}C label associated with activated ^{14}C-P directed into oxidative metabolism would be lost from the tissue (as $^{14}CO_2$) by the time of tissue sampling. The tissue ^{14}C content would therefore reflect the component of utilization directed into storage pathways (glyceride and phospholipid synthesis). Under conditions of fatty acid oxidation blockade, the metabolically sequestered ^{14}C-P would be directed into storage and therefore, in the etomoxir-treated animals, the parameter R_{fs}' would provide a reasonable estimate of the true fatty acid utilization rate (R_f). Simultaneous administration of both ^{14}C-P and ^{3}H-R-BrP enabled estimation of LC^* in individual rats in the etomoxir group using the expression

$$LC^* \approx R^*_f / R_{fs}'$$

Plasma ^{3}H-R-BrP and ^{14}C-P activity data: function fits and calculation of integrals. Integrals of the plasma activity functions, e.g., required for calculating R^*_f (equation 1) and CR_B (equation 2), were calculated analytically from parameters obtained by fitting the plasma curves to a model function (details in the Appendix).

Analysis of tissue ^{3}H retention data. To assess the assumption that metabolites of ^{3}H-R-BrP were effectively trapped, tissue ^{3}H activity at the end of the standard duration experiment (16 min) was compared to the activity at the end of an extended duration experiment (60 min). This data were then used to estimate retention over the standard 16-min experiment using procedures described in the Appendix.

Statistics

Group mean contrasts were made using analysis of variance. Comparisons made between data pairs obtained within individual animals were made using Student's paired *t*-test. Statistical calculations were performed using SPSS™ (SPSS Inc., Chicago,

Downloaded from www.jlr.org by guest, on June 14, 2012

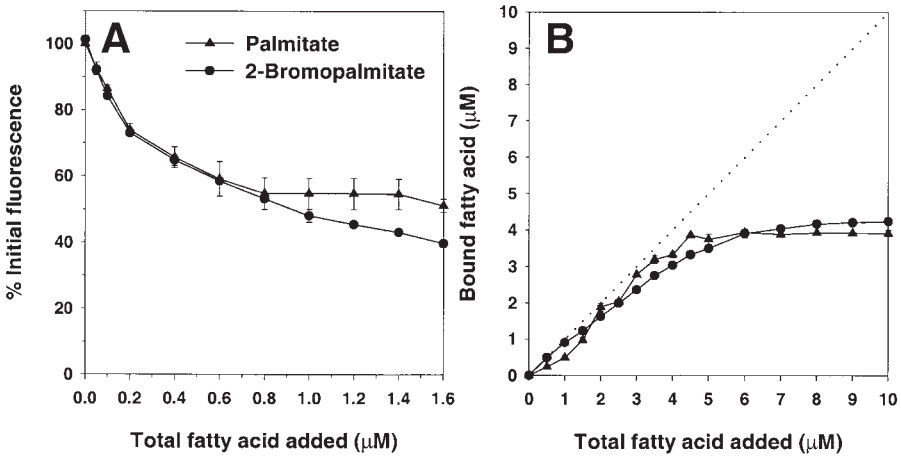

Fig. 1. Binding of 2-bromopalmitate and palmitate to intestinal fatty acid binding protein (iFABP) and bovine serum albumin (BSA). **A:** Binding to iFABP was assessed using displacement of the fluorescent probe DAUDA, from the single ligand binding site of iFABP, by the fatty acids. **B:** Binding to BSA was assessed using the reduction in intrinsic fluorescence caused by the binding of ligands to the highest affinity binding sites for long chain fatty acids.

IL). Results are reported as the mean ± SEM. *P* less than 0.05 was considered statistically significant.

RESULTS

Binding of 2-bromopalmitate and native FFA to albumin and intestinal fatty acid binding

Displacement of the fluorescent probe, DAUDA bound to iFABP, by 2-bromopalmitate and palmitate is shown in **Fig. 1A**. It has been previously established that iFABP has a single FFA binding site and that DAUDA binds to this site (28). The similar ability of the two fatty acids to displace DAUDA demonstrated that 2-bromopalmitic acid and palmitate compete for the same ligand binding site on iFABP and, furthermore, that the affinities of the two fatty acids are similar. BSA has a tryptophan at position 134 in the third structural domain whose fluorescence emission at 370 nm is quenched by bound fatty acids (19). The binding isotherms presented in Fig. 1B indicate that palmitate and 2-bromopalmitate bind to the same high affinity binding sites with similar average K_ds (2–3.5 μm) and stoichiometry.

Individual enantiomers of [9,10-^{3}H]-2-bromopalmitate as substrates for hepatic acyl CoA synthetase (ACS)

Rates of conversion of [^{14}C]palmitate, as well as the enantiomers of [9,10-^{3}H]-2-bromopalmitate to their respective CoA esters, by hepatic microsomal ACS prepared from rat liver are shown in **Fig. 2**. Of the two configurations of the bromine, only the R-enantiomer of [9,10-^{3}H]-2-bromopalmitate (^{3}H-R-BrP) was significantly activated by ACS. A decreasing rate of R-enantiomer conversion with increasing palmitate levels probably resulted from increasing competition with the unlabeled fatty acid for the enzyme. The parallel fall in ^{14}C-P conversion demonstrates that the R-enantiomer was handled by the same enzyme as the native FFA. The lower rates of conversion of the R-enantiomer indicated however that it was not as good a substrate as palmitate.

Plasma kinetics of [9,10-^{3}H]-(R)-2-bromopalmitate and [U-^{14}C]-palmitate

In vivo studies were performed with the purified ^{3}H-R-BrP, in line with the in vitro finding of stereoselectivity of ACS (above). This was done with the intention of establishing a tracer method for the determination of tissue-specific FFA utilization, where the FFA analog had to be a substrate for ACS, which metabolically sequesters native FFA.

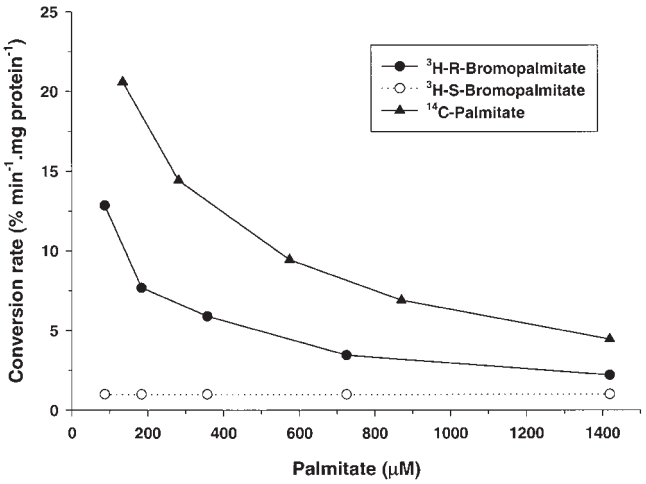

Fig. 2. Stereoselective conversion of the individual enantiomers of ^{3}H-R/S-bromopalmitate to CoA derivative by a hepatic microsomal preparation of acyl-CoA synthetase (ACS). A single representative experiment is plotted. Repeated experiments always showed the same pattern.

Downloaded from www.jlr.org by guest, on June 14, 2012

TABLE 1. Plasma labeled species distribution 16 min after the start of ^{3}H-R-BrP and ^{14}C-P infusion

	^{3}H Species			^{14}C Species	
	Polar Lipid	Neutral Lipid	^3H_2O	Polar Lipid	Neutral Lipid
Control	23.7 ± 2.1	5.4 ± 0.6	4.8 ± 1.6	12.2 ± 0.9	62.7 ± 3.5
Etomoxir	31.9 ± 2.5	3.0 ± 0.4	6.1 ± 0.4	29.5 ± 4.3	53.2 ± 4.8

Data are means ± SEM (n = 6/group). Results are expressed as % of total plasma activity. Acid lipid extractions separated lipophilic and hydrophilic species. Lipophilic species were further split into polar (free fatty acid containing) and neutral (EFA containing) subfractions using an alkaline extraction. ^3H_2O was estimated as the activity lost during evaporation of the hydrophilic fraction. Remainder of the hydrophilic fraction activity makes up the rest of the 100% of total plasma activity.

Plasma ^{3}H-R-BrP was identified using the lipid extraction–separation procedure described above. This assignment was confirmed using HPLC resolution of ^{3}H-R-BrP in two control animals. Thus, at all measurement time points, greater than 86% of the detected lipophilic species appeared under the ^{3}H-R-BrP peak (results not shown). Most of the remaining lipophilic ^{3}H activity eluted early from the column and most likely would have partitioned into the neutral lipid subfraction (see **Table 1**), therefore not influencing the measurement of ^{3}H-R-BrP activity determined in the polar lipid subfraction.

Arterial plasma tracer kinetic responses to a 4-min constant intravenous infusion of ^{3}H-R-BrP and ^{14}C-P, for the control and etomoxir-treated animals, are displayed in **Fig. 3**. During the initial tracer infusion period (0–4 min) plasma activity of both ^{3}H and ^{14}C species appeared to rapidly approach a plateau. In the period (4–16 min) after tracer infusion, plasma ^{3}H-R-BrP and ^{14}C-P levels rapidly decayed. Slower removal from plasma of ^{3}H-R-BrP than ^{14}C-P was evidenced by higher plasma levels during infusion and slower disappearance of ^{3}H-R-BrP after cessation of infusion. Plasma data for individual animals was fitted to a four parameter model function (see Appendix). Fits to group data are displayed as dotted lines in Fig. 3. Fits for all individual animals were acceptable as judged by the chi-square criteria. Parameters obtained from the fitting procedure were used to calculate plasma clearance rates of the tracers, which are shown in **Table 2**. The clearance rate estimates confirmed that the plasma clearance rate of ^{3}H-R-BrP was significantly lower than for ^{14}C-P in both the control and etomoxir-treated groups. Analysis of data pairs obtained in individual animals from either control or etomoxir-treated animals revealed a high degree of correlation between clearance rate estimates of ^{14}C-P and ^{3}H-R-BrP ($r^2 = 0.58$, $P < 0.001$), despite the fairly narrow range of the data.

Plasma FFA was increased by 67% by prior etomoxir administration compared to the control situation ($P < 0.001$, Table 2). Apparently this was not due to decreased

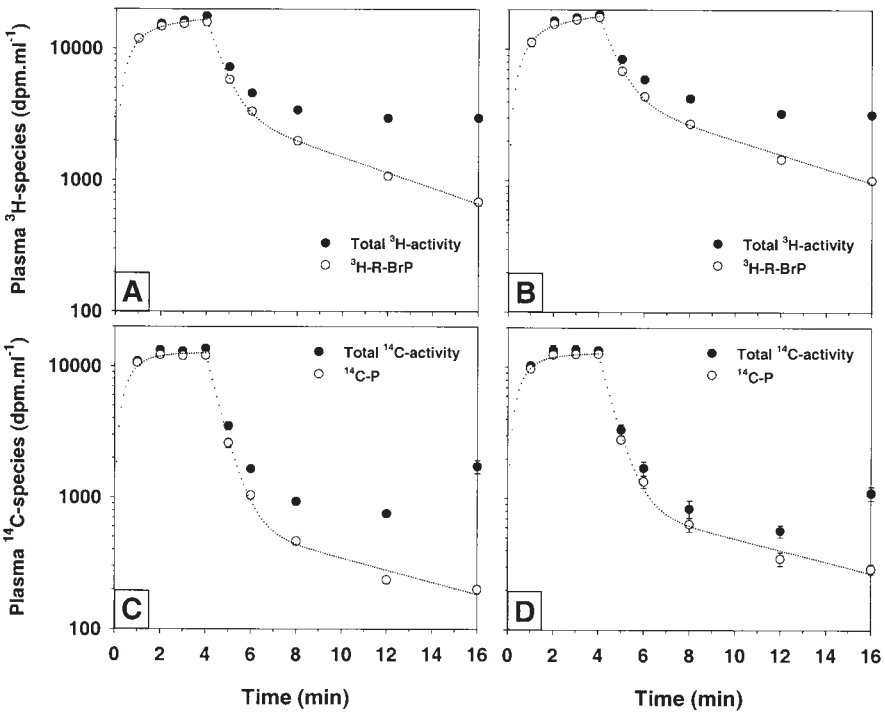

Fig. 3. Arterial plasma ^{3}H- and ^{14}C-species kinetic responses to a 4-min infusion of [9,10-^{3}H]-(R)-2-bromopalmitate (^{3}H-R-BrP) and [U-^{14}C]palmitate (^{14}C-P) complexed to bovine serum albumin. Control group data are displayed in the left hand panels (A and C), etomoxir group data in the right hand panels (B and D). Closed symbols represent total measured activities, open symbols represent the fatty acid species component (^{3}H-R-BrP or ^{14}C-P). Dotted lines denote the least-squares fits of the model function (see Appendix) to the fatty acid species data. Data have been normalized to infusion rates of 0.25×10^6 dpm·min^{-1} for both tracers and a body weight of 350 g.

Downloaded from www.jlr.org by guest, on June 14, 2012

TABLE 2. Plasma FFA and whole body parameters derived from plasma ^{3}H-R-BrP and ^{14}C-P tracer kinetics

	Control	Etomoxir
Plasma FFA (mm)	0.42 ± 0.03	0.70 ± 0.08[b]
Plasma insulin (pm)	265 ± 30	250 ± 70
Plasma glucose (mm)	8.3 ± 0.3	7.0 ± 0.3[a]
Plasma clearance rate of ^{3}H-R-BrP ($ml \cdot kg^{-1} min^{-1}$)	31.6 ± 1.5[c]	28.0 ± 1.2[c]
Plasma clearance rate of ^{14}C-P ($ml \cdot kg^{-1} min^{-1}$)	49.9 ± 2.6	47.4 ± 1.9
Distribution volume of ^{3}H-R-BrP ($ml \cdot kg^{-1}$)	28.1 ± 3.0	34.0 ± 1.9
Distribution volume of ^{14}C-P ($ml \cdot kg^{-1}$)	31.9 ± 3.8	35.6 ± 1.8

Data are means ± SEM (n = 6) for an untreated control group and a group given etomoxir (20 $\mu mol \cdot kg^{-1}$), as a bolus 25 min before tracer administration.

[a] $P < 0.05$; [b] $P < 0.001$ vs. control group.

[c] $P < 0.001$ vs. ^{14}C-P.

plasma FFA clearance, as clearance rate estimates of neither ^{14}C-P nor ^{3}H-R-BrP were significantly reduced by etomoxir. We suggest that the failure of etomoxir to significantly lower plasma FFA clearance was due to the predominantly non-oxidative metabolism of FFAs at the whole body level under the conditions of the present study, i.e., barbiturate anesthesia. This conclusion is supported by the tissue-specific data (below) indicating large etomoxir-induced reductions of FFA clearance only in tissues where we would be confident that a major metabolic fate of FFAs was oxidation (contracting muscles). As no reduction of plasma FFA clearance was detected, it can be inferred that the elevated plasma FFA concentrations were due to increased rates of appearance of FFA into plasma (R_a). Plasma glucose and insulin levels (Table 2) were measured to assess their potential role in this etomoxir-induced increase in R_a. While insulin concentrations were not altered, etomoxir did lower plasma glucose levels which may have contributed to the increased FFA mobilization via a reduction in adipose tissue re-esterification. Possible involvement of counter-regulatory hormones was not investigated.

Appearance of radiolabeled metabolites in plasma

At the earliest (1 min) time point, virtually all of the ^{14}C and ^{3}H activity was associated with ^{14}C-P and ^{3}H-R-BrP, respectively (Fig. 3). Appearance of labeled, non-free fatty acid species, progressively reduced the relative contribution of the ^{14}C-P and ^{3}H-R-BrP to total plasma ^{3}H and ^{14}C activity with increasing time. The nature of the labeled ^{3}H and ^{14}C metabolites was, however, quite different. At late time points the disappearance of total ^{14}C activity reversed and activity increased (beginning 12–16 min, Fig. 3). This pattern has been observed previously (29) and most likely represents ^{14}C-P that has been taken up by the liver, esterified, and subsequently exported in VLDL particles. This interpretation was supported by our analysis of the final (16 min) plasma sample showing that most of the non-^{14}C-P material appears in the non-polar lipid-extractable fraction (Table 1). In contrast to ^{14}C species kinetics, total ^{3}H activity decayed towards a plateau at late time points (Fig. 3) and as the ^{3}H-labeled metabolite was hydrophilic (Table 1) it could not have been associated with esterified ^{3}H-R-BrP.

The appearance of only small amounts of ^3H_2O (identified using evaporation) in the plasma at 16 min (Table 1) confirmed the expectation that oxidative metabolism was a minor metabolic fate of ^{3}H-R-BrP. Assuming a body water content of 70% of body weight and complete equilibrium of ^3H_2O among all body water compartments at 16 min, it was estimated that of the total administered ^{3}H-R-BrP a maximum of only 4 ± 1% in control and 5 ± 1% in etomoxir-treated rats was oxidized to ^3H_2O.

Tissue metabolites of ^{3}H-R-BrP

A necessary condition required for equation 1 to provide an accurate estimate of R^*_f is that at the tissue sampling time (16 min) the contribution of unmetabolized ^{3}H-R-BrP to total tissue ^{3}H activity be small (see Appendix). We assessed this condition using an HPLC analysis of extracts of tissues obtained under standard conditions (16 min, etc.) from two control animals. Results of this analysis confirmed that only a small fraction of tissue activity was unmetabolized ^{3}H-R-BrP. Individual tissue results expressed as percentage of total recovered ^{3}H activity appearing under the ^{3}H-R-BrP peak were: WQ 11%, RQ 10%, heart 8%, and liver <1%. The ^{3}H labeled metabolites are yet to be identified.

Tissue-specific indices of plasma FFA metabolism

Table 3 and **Fig. 4** show indices of FFA utilization (R^*_f) and the component of FFA utilization directed into storage metabolism (R_{fs}') which were calculated from total ^{3}H and ^{14}C activities in tissues collected 16 min after the start of tracer infusion, as well as areas under the plasma ^{3}H-R-BrP and ^{14}C-P curves using equations 1 and 3, respectively. Etomoxir was administered to block fatty acid oxidation, thereby forcing the tissues into a predominantly storage mode of fatty acid metabolism. As expected, etomoxir increased R_{fs}' in most of the tissues examined. Etomoxir-induced changes in R^*_f differed from tissue to tissue, however, probably reflecting the combined influence of the elevation in systemic FFA (Table 2) and differences in the metabolic status of the individual tissues in the control group. Thus, in tissues likely to oxidize a large fraction of metabolically sequestered FFAs in the control animals (heart, diaphragm [Table 3] and contracting hindlimb muscles [Fig. 4]), etomoxir either significantly decreased or did not change R^*_f compared to the untreated controls. By contrast, in those tissues likely to be in a storage mode of FFA metabolism (brain, WAT [Table 3] and non-contracting hindlimb muscles [Fig. 4]), etomoxir increased R^*_f.

As noted above, etomoxir increased systemic FFA levels, which on its own could increase tissue FFA utilization, through simple mass action. To exclude the effect of this etomoxir-induced increase in FFA and isolate the local tissue level effects of etomoxir on FFA uptake, indices of tissue-specific clearance of FFA (K^*_f) were calculated from the R^*_f and plasma FFA (C_P) data as $K^*_f = R^*_f / C_P$. In oxida-

Downloaded from www.jlr.org by guest, on June 14, 2012

TABLE 3. Indices of fatty acid utilization (R^*_f) and fatty acid incorporation into storage (R_{fs}') in individual tissues

	Control			Etomoxir		
	R^*_f	R_{fs}'	R^*_f / R_{fs}'	R^*_f	R_{fs}'	R^*_f / R_{fs}'
Heart	12.4 ± 1.3	5.0 ± 0.6	2.65 ± 0.38	3.4 ± 0.2[c]	18.3 ± 1.1[c]	0.19 ± 0.01[c]
Leg muscles						
Non-stim	Fig. 4A	Fig. 4C	0.37 ± 0.01	Fig. 4B	Fig. 4D	0.39 ± 0.02
Contracting	Fig. 4A	Fig. 4C	0.95 ± 0.05	Fig. 4B	Fig. 4D	0.36 ± 0.01[c]
Diaphragm	1.8 ± 0.2	2.7 ± 0.3	0.68 ± 0.04	1.6 ± 0.1	5.2 ± 0.6[b]	0.32 ± 0.02[c]
WAT	0.35 ± 0.03	0.90 ± 0.10	0.40 ± 0.01	0.64 ± 0.03[b]	1.89 ± 0.31[b]	0.38 ± 0.03
Kidney	3.3 ± 0.3	5.2 ± 0.6	0.65 ± 0.04	3.8 ± 0.4	8.3 ± 0.9[a]	0.47 ± 0.03[b]
Brain	0.20 ± 0.02	0.38 ± 0.04	0.52 ± 0.02	0.36 ± 0.05[a]	0.53 ± 0.07	0.67 ± 0.02[c]
Liver	20.1 ± 2.2	19.8 ± 2.8	1.04 ± 0.09	27.0 ± 2.8	36.7 ± 5.4[a]	0.76 ± 0.03[a]
BAT	2.5 ± 0.2	2.8 ± 0.2	0.88 ± 0.05	5.3 ± 1.1[a]	6.9 ± 1.7	0.80 ± 0.03

Data are given as μmol of plasma FFA utilized per 100 g tissue per minute. Hindlimb muscles are categorized as either control (Non-stim) or sciatic nerve electrically stimulated (Contracting); see Fig. 4 for individual muscle results. White adipose tissue (WAT) results represent an average of values from epididymal and inguinal depots. Brown adipose tissue (BAT) was taken from the interscapular depot.

[a] $P < 0.05$, [b] $P < 0.01$, [c] $P < 0.001$ vs. control group.

tive tissues, K^*_f estimates were reduced by etomoxir (heart 30.9 ± 0.9 vs. 5.2 ± 0.8; diaphragm 4.5 ± 0.3 vs. 2.3 ± 0.1; contracting WG 2.9 ± 0.2 vs. 0.9 ± 0.1; contracting RG 2.9 ± 0.3 vs. 1.7 ± 0.1; contracting EDL 4.1 ± 0.4 vs. 1.1 ± 0.1 ml·min^{-1}·100 g^{-1}; Control vs. Etomoxir, $P < 0.01$) with no change in non-oxidative tissues (brain 0.50 ± 0.04 vs. 0.50 ± 0.03; WAT 0.88 ± 0.05 vs. 0.88 ± 0.07; non-contracting WG 0.83 ± 0.06 vs. 0.82 ± 0.06; non-contracting RG 1.3 ± 0.1 vs. 1.5 ± 0.1; non-contracting EDL 1.0 ± 0.1 vs. 1.1 ± 0.1 ml·min^{-1}·100 g^{-1}; Control vs. Etomoxir, $P > 0.05$). The tissue R^*_f results are therefore clearly consistent with the expected action of etomoxir to block FFA oxidation.

Hindlimb skeletal muscle R_f and R_{fs}' results are presented in Fig. 4. First, looking at only the resting leg muscles, we note that the R^*_f (and R_{fs}') values for the various muscles rank: principally oxidative muscles (RQ, RG) > mixed muscle (EDL) > principally glycolytic muscles (WG,

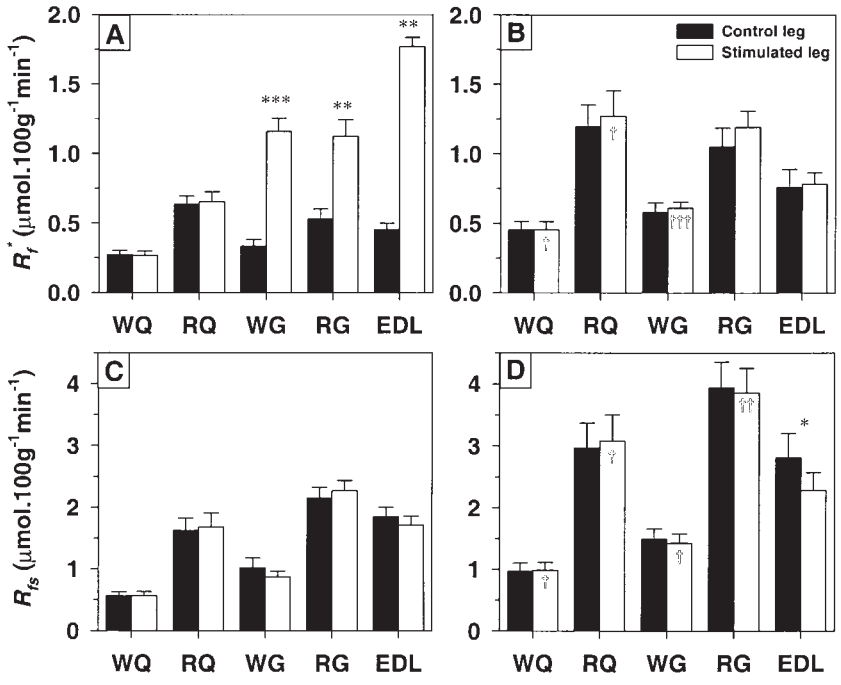

Fig. 4. Effect of contraction and etomoxir on indices of fatty acid utilization (R^*_f) and fatty acid storage (R_{fs}') in individual hindlimb muscles: white quadriceps (WQ); red quadriceps (RQ); white gastrocnemius (WG); red gastrocnemius (RG); extensor digitorum longus (EDL). Control group data are shown in the left hand panels (A and C), etomoxir group data in the right hand panels (B and D). Unilateral sciatic nerve stimulation elicited muscle contractions in the lower leg muscles (WG, RG, EDL) of the stimulated side. Closed histograms represent muscles on the control side, open histograms the stimulated side. *$P < 0.05$, **$P < 0.01$, ***$P < 0.001$ vs. control leg. †$P < 0.05$, ††$P < 0.01$, †††$P < 0.001$ vs. control group.

Downloaded from www.jlr.org by guest, on June 14, 2012

WQ). Unilateral sciatic nerve stimulation elicited contraction only in the lower leg muscles (WG, RG and EDL) of the stimulated side. Consistent with this (panel A), a large contraction-induced increase in R^*_f was observed in all three lower leg muscles with no change in R^*_f in the quadriceps muscles (WQ and RQ) of the thigh of the stimulated side, compared with the control side. By contrast, muscle contraction had no apparent effect on R_{fs}' (panel C); values for individual muscles, including WG, RG, and EDL, were the same in the stimulated and control legs. These results indicated that muscle contraction induced an increase in fatty acid uptake and utilization, which was directed selectively into oxidative metabolism. This interpretation was reinforced by the hindlimb muscle responses obtained in the etomoxir-treated group (panels B and D). β-Oxidation blockade completely abolished the contraction-induced increases in R^*_f in WG, RG, and EDL; values for all hindlimb muscles were similar in stimulated and control legs. No differences in R_{fs}' were seen between the stimulated and control legs except in EDL where there was a small but statistically significant reduction in the stimulated side.

The R^*_f / R_{fs}' ratios in the etomoxir treatment group (Table 3) provided estimates of the lumped constant (LC^*) for ^{3}H-R-BrP. For all tissues examined, the R^*_f / R_{fs}' ratios were significantly less than 1 ($P < 0.01$), indicating slower uptake or metabolism of ^{3}H-R-BrP than ^{14}C-P. In addition to assessing treatment-induced changes in individual tissue R^*_f values, it would be generally useful to be able to compare the R^*_f values of different tissues. To do this directly, the lumped constants for the tissues being compared should be similar. To assess the variability of LC^* across different tissues, multiple range comparisons (Student-Newman-Keuls test [30]) were conducted to compare mean etomoxir group R^*_f / R_{fs}' values for different tissues in Table 3. The test indicated that ratios for heart, brain, liver, and BAT were not compatible with ratios for skeletal muscles, WAT, and kidney (results not shown).

Retention of tissue ^{3}H and ^{14}C activity

The effectiveness of tissue trapping of ^{3}H-labeled metabolites of ^{3}H-R-BrP was assessed by evaluating the reduction in tissue ^{3}H activity over an extended duration experiment. Increasing the experimental duration from 16 min to 60 min revealed loss of total ^{3}H activity from all tissues except brain (**Table 4**). First order rate constants (λ), calculated from the ratios of ^{3}H activity at 60 min to 16 min, were used to estimate the retention of ^{3}H activity over the standard 0–16 min experiment. Relatively low rates of loss were estimated in hindlimb muscles, diaphragm, WAT, BAT, and kidney (8–23%/16 min). Higher rates of ^{3}H loss were apparent in the heart (35%/16 min) and liver (30%/16 min). It should be pointed out that these estimates are based on the assumption that all of the ^{3}H-R-BrP is present in the tissues at the time of the start of the ^{3}H-R-BrP infusion. Thus the calculated rates of loss will be overestimated. The metabolic status of a particular tissue apparently did not influence ^{3}H retention as indicated by the lack of difference between retentions in contracting and non-contracting hindlimb muscles (compare results for WG, RG, and EDL, Table 4).

Unlike ^{3}H-R-BrP, which undergoes very little oxidation over the 16-min experiment (above), ^{14}C-P is readily oxidizable. The $^{14}CO_2$ produced would be rapidly lost from the tissues and eliminated from the animal. As most of the infused ^{14}C-P has left the plasma by 16 min and because of the rapidity of FFA oxidation, it is reasonable to expect

TABLE 4. Retention of tissue ^{3}H and ^{14}C activity after intravenous administration of ^{3}H-R-BrP and ^{14}C-P

	^{3}H Activity			^{14}C Activity		
	Ratio 60 Min/16 Min	λ	16 Min Retention	Ratio 60 Min/16 Min	λ	16 Min Retention
	%	min^{-1}	%	%	min^{-1}	%
Heart						
Leg muscles						
Non-stim						
WQ	69 ± 10	0.0085	87	86 ± 11	0.0035	95
RQ	62 ± 7	0.0110	84	96 ± 8	0.0010	98
WG	73 ± 7	0.0073	89	79 ± 8	0.0054	92
RG	65 ± 8	0.0102	85	90 ± 9	0.0025	96
EDL	74 ± 11	0.0071	89	87 ± 8	0.0032	95
Contracting						
WG	80 ± 4	0.0053	92	80 ± 8	0.0051	92
RG	77 ± 12	0.0061	91	85 ± 7	0.0037	94
EDL	64 ± 11	0.0103	85	82 ± 5	0.0047	93
Diaphragm	49 ± 6	0.0164	77	94 ± 11	0.0015	98
WAT	54 ± 4	0.0142	79	64 ± 8	0.0104	84
Kidney	58 ± 3	0.0126	82	75 ± 5	0.0067	90
Brain	119 ± 6	−0.0040	107	109 ± 11	−0.0021	103
Liver	38 ± 5	0.0224	70	54 ± 3	0.0145	79
BAT	78 ± 14	0.0057	91	169 ± 41	−0.0122	122

Tissue activities were determined in separate groups with tissues collected at either 16 min or 60 min after commencement of tracer infusion. Ratio data represents 60 min activities divided by the mean 16 min activity, after dose normalization. First order rate constants for loss of activity (λ) were calculated from this ratio and used to estimate the fraction of label retained in tissues over the standard experimental time of 16 min (16 min Retention).

Downloaded from www.jlr.org by guest, on June 14, 2012

that the majority of ^{14}C activity remaining in the tissue at 16 min was derived from non-oxidative (storage) metabolism. From 16 min, the reduction of ^{14}C activity in most tissues was slow; only in liver was the estimated loss >20%/16 min (Table 4). Stability of the ^{14}C-labeled products at 16 min was further emphasized by the apparent lack of effect of muscle contraction status (and hence oxidative metabolism) on ^{14}C retention, i.e., estimated 16 min retentions in contracting and non-stimulated hindlimb muscles were the same.

DISCUSSION

We describe a new method for the determination of tissue-specific rates of free fatty acid (FFA) utilization in vivo. The method is based on the use of [9,10-^{3}H]-2-bromopalmitate, a synthetic partially metabolizable fatty acid tracer. A prerequisite was that this tracer would qualitatively participate in the same transport and metabolic sequestration steps as those that handle native FFAs. Consistent with this, our in vitro studies confirmed that 2-bromopalmitate and palmitate compete for the same ligand binding sites on extracellular and intracellular fatty acid binding proteins. We found, however, that the initial intracellular activation reaction, catalyzed by the enzyme acyl-CoA synthetase (ACS), was stereoselective for one isomer, [9,10-^{3}H]-(R)-2-bromopalmitate (^{3}H-R-BrP). A procedure was developed for the in vivo determination of an index of tissue-specific FFA utilization, which we have called R^*_f, based on the local entrapment of ^{3}H-labeled products in tissue samples collected 16 min after the start of a 4-min intravenous infusion of ^{3}H-R-BrP. The basic principle was that after transfer of plasma ^{3}H-R-BrP to the cells, transport across the plasma membrane into the cytosol, and activation by ACS, a ^{3}H-labeled product would be formed which would be metabolically trapped and retained in the tissues. Ideally the tissue ^{3}H-labeled product content at the time of tissue sampling would represent the integral of all ^{3}H-R-BrP flux through the ACS reaction. Under these circumstances R^*_f would be proportional to the native FFA activation rate. The proportionality, or "lumped" constant (LC^*) represents the ratio of the likelihood that a molecule of plasma ^{3}H-R-BrP will be activated to ^{3}H-R-BrP-CoA to the likelihood that a molecule of plasma FFA will undergo activation to its CoA derivative.

In vivo experiments were conducted to address the validity of the method, assessing specific assumptions including the tissue-specific effectiveness of ^{3}H-labeled product trapping. Satisfactory levels of ^{3}H retention were observed in most tissues. Comparison of R^*_f, and an index of the rate of FFA incorporation into storage products (R_fs'), obtained from the kinetics of a simultaneously administered radiolabeled native FFA, [U-^{14}C]palmitate (^{14}C-P), under conditions of pharmacological fatty acid oxidation blockade by etomoxir, enabled estimation of LC^*. This analysis revealed that bromination of the palmitate molecule does significantly slow tissue uptake from plasma or its subsequent metabolism (such that $LC^* < 1$). The present results demonstrate that the parameter R^*_f reliably indexes changes in total fatty acid utilization (including oxidative and non-oxidative metabolism) in a range of metabolically important tissues, notably skeletal muscles and fat.

Validity of R^*_f as an estimate of tissue-specific plasma FFA utilization rate

The theoretical basis for the derivation of the equation 1 for R^*_f is outlined in the Appendix, and a more complete treatment of the derivation of equations for the general analogous problem, where a partially metabolizable analog of a natural substance is used to estimate the reaction velocity of the native substance, is given in ref. 31. Briefly, the major assumptions are: *1*) that ^{3}H-R-BrP participates in the same transport and metabolic sequestration processes as native FFAs; *2*) that the ^{3}H-labeled products of the analog are metabolically trapped and; *3*) that the analog does not influence native FFA metabolism (the trace amount assumption). It is noteworthy that there is no theoretical requirement for LC^* (the proportionality constant between R^*_f and the true fatty acid utilization rate) to be a particular value, e.g., 1. Evidence concerning the validity of the major assumptions is considered below.

Assumption 1: ^{3}H-R-BrP competes for the same transport and metabolic sequestration steps as native FFAs. The protein binding studies indicated satisfaction of the basic requirement that 2-bromopalmitate would trace the extracellular and intracellular transport of native FFAs. Thus, 2-bromopalmitate and palmitate bound with similar affinity and stoichiometry to the same high affinity ligand binding sites on iFABP and albumin (Fig. 1).

Stereoselectivity of the ACS enzyme for 2-bromopalmitate (Fig. 2) suggested that the individual isomers would exhibit very different kinetics in vivo, and that only the activatable R-isomer (^{3}H-R-BrP) would be useful as a tracer of FFA utilization. This followed because the ACS-mediated activation step is required for commitment of FFA to the major pathways of fatty acid metabolism. The present findings are consistent with previous reports of stereoselectivity of ACS for other compounds (32, 33).

In line with the in vitro finding of stereoselectivity of the ACS enzyme, our in vivo method for the assessment of tissue-specific FFA utilization is based on the administration of pure ^{3}H-R-BrP. Chemistry used for the synthesis of the analog took advantage of commercially available high specific activity [9,10-^{3}H]palmitate as starting material. The bromination step produced a racemic mixture of enantiomers. A method was therefore developed for resolution of the individual enantiomers, described in detail elsewhere (24).

Assumption 2: Metabolic trapping. At the whole body level, the production of only very small amounts of ^3H_2O (<5% ^{3}H dose) confirmed the fundamental requirement that oxidative metabolism was a minor metabolic fate of ^{3}H-R-BrP. The much lower emergence of ^{3}H-labeled neutral lipid species in the plasma, compared with ^{14}C-labeled species, suggested that ^{3}H-R-BrP is also a very poor substrate for esterification. Potential errors resulting from recirculation of esterified ^{3}H-R-BrP in VLDL would therefore most likely be minimal. At the individual tissue level,

Downloaded from www.jlr.org by guest, on June 14, 2012

acceptable levels of trapping of ^{3}H-labeled metabolites of ^{3}H-R-BrP were estimated in most tissues over the standard experimental period of 16 min (Table 4). Relatively slow rates of loss of ^{3}H activity from brain, brown adipose tissue, skeletal muscles, kidney, white adipose tissue, and diaphragm imply reasonably accurate determination of R^*_f. It was also noteworthy that in hindlimb muscles the contraction status, and hence presumably the metabolic status (oxidation versus storage metabolism), had no apparent effect on retention. In contrast to the majority of tissues, substantial rates of ^{3}H loss were observed in liver (30%/16 min) and heart (35%/16 min), degrading the reliability of R^*_f estimates for these tissues.

The fairly rapid loss of ^{3}H activity from some tissues suggested shortening the experiment from 16 min, in order to increase the accuracy of R^*_f estimates, e.g., if the experiment were terminated at 12 min instead, the estimated losses would be 23% in liver and 27% in heart. Another motive for shortening the experiment relates to the progressive appearance in plasma of the hydrophilic ^{3}H-labeled metabolite (Fig. 3). Arguing against a shorter experiment would be that errors arise from the increased inclusion of free ^{3}H-R-BrP in the measured total tissue ^{3}H activity. This includes ^{3}H-R-BrP both in the circulation and in the cells that would subsequently escape metabolic sequestration, returning to the circulation. As mentioned above, we found that at 16 min the contribution of nonmetabolized ^{3}H-R-BrP was minor, less than 12% in the tissues examined.

Identification of the tissue and plasma metabolites of ^{3}H-R-BrP remains an important task for future work. This could provide further insight into the robustness of the technique and allow prediction of situations where the method may fail. While β-oxidation does not appear possible for 2-bromopalmitate (17), other pathways of oxidative metabolism, particularly ω-oxidation would theoretically not be prevented by the bromine on the alpha carbon. While ω-oxidation is unlikely to be a quantitatively important pathway for FFA metabolism under ordinary circumstances, situations may arise, e.g., treatment with peroxisome proliferators, where enhanced ω-oxidation in some tissues, notably the liver, would result in accelerated rates of local ^{3}H activity loss and hence less accurate R^*_f estimates.

Assumption 3: trace amount. A fundamental requirement for a metabolic tracer to be useful is that it does not perturb the metabolic system under study. Pharmacologically, 2-bromopalmitate has been used to block β-oxidation, possibly via an almost irreversible interaction of 2-bromopalmitoyl-CoA with CPT I (18). To assess the potential perturbation of the 2-bromopalmitate administered in our experiments, we have calculated the extent of CPT I inhibition based on average tissue ^{3}H levels at 16 min and assuming that all tissue ^{3}H activity was associated with ^{3}H-R-BrP-CoA, irreversibly bound to the palmitoyl-CoA binding site of CPT I. Using CPT I binding capacities from Declercq et al. (34), we estimate that the administration of a large dose of 425 pM (50×10^6 dpm) ^{3}H-R-BrP would inhibit 5% and 17% of the total CPT I content in red quadriceps muscle and liver, respectively. As this analysis is based on the worst case scenario, we believe it is unlikely that the ^{3}H-R-BrP tracer had any significant impact on FFA oxidation. At the same time, this analysis provides clear motivation for synthesis of high specific activity (R)-2-bromopalmitate tracer.

Determination of tissue-specific plasma FFA utilization rate R^*_f

Our method culminates in the calculation of the parameter R^*_f, which is an index of tissue-specific fatty acid utilization rate. Calculation of R^*_f (equation 1) requires estimation of the following three variables. *1) Plasma FFA concentration*. Implicit in the use of total FFA for this calculation is the assumption that all native FFA species have kinetically identical behavior. The basic rationale for the current use of an analog of palmitate, rather than another long chain FFA derivative, is that palmitate is one of the most abundant plasma FFA species. Measurement of FFA level requires that heparin is not used. In the current experiments, Na_3-citrate was applied for maintaining sampling catheter patency. The ^{3}H-R-BrP and ^{14}C-P tracers were complexed to albumin for infusion. To increase the likelihood that the kinetics of these tracers would reflect the transfer kinetics of the bulk plasma FFA, which is distributed among several albumin binding sites of different affinities and off-rates, the following procedure was adopted. Tracers were randomized with unlabeled FFA by mixing them together with unlabeled palmitate before complexing to FFA-free albumin in a palmitate:albumin molar ratio of 0.76. This ratio was chosen to approximate the expected in vivo plasma molar ratios, based on plasma FFA levels around 0.5 mm. *2) Tissue content of ^{3}H product*. With the aim of developing a straightforward and accurate method for routine tissue processing, we used total tissue ^{3}H activity as a surrogate measure of the ^{3}H-labeled metabolites of ^{3}H-R-BrP. Justification for this simplified approach was obtained from a detailed chromatographic analysis of tissue ^{3}H-labeled metabolites which showed that less than 12% of recovered tissue ^{3}H activity was associated with unmetabolized ^{3}H-R-BrP. *3) Plasma ^{3}H-BrP activity*. To determine the area under the plasma ^{3}H-R-BrP activity curve, plasma processing methods were required for resolving ^{3}H-R-BrP from hydrophilic radiolabeled products which appeared in the plasma over the course of the experiment. We identified ^{3}H-R-BrP (and ^{14}C-P) as the material contained in the polar species subfraction of a lipid extract (see Methods).

Validity of R_{fs}' as an estimate of the non-oxidative component of FFA utilization rate

The tissue ^{14}C retention data indicated R_{fs}' as a valid estimate of the rate of fatty acid incorporation into storage. Unlike ^{3}H-R-BrP, which does not undergo significant oxidation over the 16-min experiment, ^{14}C-P is readily oxidizable. After activation by ACS, ^{14}C-P is committed either to oxidative or storage metabolism. Independence of these pathways is strongly supported by recent, very elegant tracer studies showing that fatty acids which enter the cells destined to be oxidized are transported directly into the mitochondria,

Downloaded from www.jlr.org by guest, on June 14, 2012

without transiting a premitochondrial glycerolipid pool (35). The basic assumption required for the calculation of R_{fs}' is that the tissue ^{14}C activity (at the time of tissue sampling) represents the integral of all ^{14}C-P flux directed into non-oxidative metabolism over the 16-min experiment (equation 3). For this to be true, the ^{14}C-labeled products of non-oxidative ^{14}C-P metabolism must be effectively trapped, a condition that should be facilitated by the relatively large intracellular pool sizes of the major storage products of FFAs, glycerides and phospholipids. An additional requirement is that ^{14}C-P entering oxidative metabolism must be completely oxidized to $^{14}CO_2$ and lost from the tissues before 16 min. Satisfactory fulfillment of these requirements was indicated by the effective retention of ^{14}C label present in the tissues at 16 min, as indicated by the slow rates of loss of ^{14}C activity between 16 and 60 min (Table 4).

It should be pointed out that the simple method of estimating R_{fs}' here does not take into account the possibility of significant ^{14}C label fixation from $^{14}CO_2$ via TCA cycle exchange reactions (a problem referred to previously (35)) which could falsely elevate R_{fs}'. It was, however, encouraging that sustained twitch contractions in skeletal muscle, which would be expected to increase local oxidative ^{14}C-P metabolism and reduce TCA exchange reactions, had absolutely no effect on ^{14}C retention. This suggests a minimal contribution of ^{14}C label derived from oxidative metabolism to the ^{14}C activity at 16 min and emphasizes the effectiveness of trapping of ^{14}C-labeled products of non-oxidative metabolism, even in the presence of high rates of oxidative metabolism.

Relationship between R^*_f and the true FFA utilization rate: the lumped constant (LC^*)

R^*_f should be interpreted as an indirect index of FFA utilization rate, rather than a direct measure of absolute FFA utilization rate. To establish a reference point for the present results, we note that the ideal FFA analog would have kinetics quantitatively identical to native FFA for all initial transport and metabolic sequestration steps. In this case $LC^* = 1$, and R^*_f would represent a direct measure of FFA utilization rate. In contrast to this ideal at the whole body level, we observed slower removal of intravenously administered ^3H-R-BrP from plasma than simultaneously administered ^{14}C-P (Fig. 3). Calculation of whole body lumped constants (from the ratio of the estimated plasma clearance rates of ^3H-R-BrP and ^{14}C-P in both the control and etomoxir-treated groups [Table 2]) indicated an "average" tissue LC^* of 0.62 ± 0.03. Whether the whole body kinetics reflected a generally slower handling of ^3H-R-BrP by tissues or, alternatively, was dominated by the influence of a small subset of the body's tissues, could only be resolved through a tissue-specific approach.

The inclusion of the etomoxir treatment group created a situation where LC^* values for individual tissues could be estimated in vivo. Information about tissue-specific rates of native FFA utilization was obtained from the parameter R_{fs}', our estimate of the component of fatty acid utilization that is directed into storage, which is based on the tissue retention of ^{14}C-labeled products of ^{14}C-P. The idea was that if β-oxidation blockade could be effected using a high dose of etomoxir (20 $\mu mol \cdot kg^{-1}$), then all activated ^{14}C-P would be directed into storage pathways and retained until tissue collection. Under these special circumstances, R_{fs}' would provide an estimate of the true fatty acid utilization rate. Estimates of LC^* could then be obtained from the R^*_f / R_{fs}' ratios in the etomoxir-treated animals. A comparison of the R^*_f / R_{fs}' ratios in the control and etomoxir-treated animals (shown in Table 3) proved that this approach was successful. Significant levels of fatty acid oxidation would be expected to increase the ratio through a relative reduction of the denominator R_{fs}'. Compatible with this expectation, ratios were generally higher in the control group, particularly in those tissues likely to have significant levels of oxidative metabolism, e.g., contracting hindlimb muscles and heart. In contrast, etomoxir had little effect on the R^*_f / R_{fs}' ratio in tissues likely to be in a predominantly non-oxidative mode of metabolism (e.g., non-stimulated hindlimb muscles and white adipose tissue).

The tissue data demonstrated a generally slower uptake and/or metabolism of ^3H-R-BrP than ^{14}C-P across a range of tissues, resulting in lumped constant (LC^*) estimates less than unity. Skeletal muscles and white adipose tissue LC^* estimates were similar ~0.38 (Table 3), indicating genuine FFA utilization rates of $\sim 2.7 \times R^*_f$. For comparison, lumped constants for the deoxyglucose analogs, widely used for assessing tissue specific rates of glucose utilization, have mean values of ~0.46 in brain (9) and estimates in heart range from 0.33 upwards (36). Some heterogeneity of R^*_f / R_{fs}' ratios across different tissues was observed, which may have been at least partly due to incomplete tissue retention of either the ^{14}C or the ^3H label, rather than regional differences in the relative rates of handling of the analog and the native FFA. Thus the higher R^*_f / R_{fs}' ratios in liver and BAT could be explained by significant levels of non-mitochondrial fatty acid oxidation in these particular tissues, which would not be blocked by etomoxir (37). Under these circumstances, $^{14}CO_2$ would be lost from the tissues during the 16-min experiment which would lower the denominator of the ratio. The low R^*_f / R_{fs}' ratio in heart is partly explainable by the comparatively high rate of loss of ^3H from this tissue (referred to above). Thus, if corrections are made for the ^3H (and ^{14}C) losses using the rate constants in Table 4, the R^*_f / R_{fs}' ratio increases from 0.19 to 0.25.

The usefulness of R^*_f estimates for individual tissues will ultimately depend on the robustness of the tissue LC^* across different physiological states and treatments. Revealing the processes responsible for the low LC^* may provide some basis for predicting this robustness. Bromination could theoretically reduce the transport rate of palmitate either through the influence of increased molecular size or decreased hydrophobicity. Alternatively, reduced rates of transport of the analog could result from high affinity binding with plasma albumin or FABP, but the binding studies suggested similar affinities of the analog and natural fatty acid (Fig. 1). The in vitro work did, however, indicate one possible explanation for the low lumped constant, namely a slower rate of activation by the enzyme

Downloaded from www.jlr.org by guest, on June 14, 2012

ACS (Fig. 2). Finally, it is worth pointing out that the magnitude of the lumped constants obtained here for ^{3}H-R-BrP, as well as the interpretation given to the parameter R^*_f, are in fact very similar to the analogous, widely used method for estimating local rates of glucose metabolism based on the use of 2-deoxyglucose tracer (9).

Indices of tissue-specific fatty acid metabolism, R_{fs}' and R^*f, trace fatty acid storage, and utilization

The pattern of R^*_f responses observed in skeletal muscle demonstrated that, at a qualitative level at least, ^{3}H-R-BrP reliably traced total native FFA utilization (Fig. 4). First, in the non-contracting hindlimb muscles, we observed that both R^*_f and R_{fs}' ranked according to the oxidative capacity of the different muscle types. Most compelling was that sustainable contractions induced substantial increases in R^*_f, without any increase in R_{fs}', indicating that contraction induced an increase in fatty acid utilization that was directed selectively into oxidative metabolism. Thus R^*_f traced total fatty acid utilization, including oxidative metabolism, while R_{fs}' traced fatty acid storage. This interpretation was greatly reinforced by the observation that β-oxidation blockade completely abolished the contraction-induced increases in R^*_f.

Further evidence that ^{3}H-R-BrP traced total fatty acid utilization at a more general tissue level was obtained by an analysis of the effects of etomoxir on R^*_f and R_{fs}' results in all tissues (results in Table 3). The contention was that if ^{3}H-R-BrP traced plasma FFA metabolism, then effects of etomoxir on R^*_f would be expected to differ from tissue to tissue, depending on the extent of fatty acid oxidation within individual tissues. Where the major metabolic fate of plasma FFA was β-oxidation, etomoxir should have decreased fatty acid utilization and hence R^*_f. This would be expected to occur through an accumulation of cytosolic fatty acyl-CoA, leading to product inhibition of ACS and hence reduced sequestration of FFA. In those tissues where storage was the major fate, etomoxir should have increased R^*_f, because of the observed etomoxir-induced increase in plasma FFA (Table 2). Between these extremes, etomoxir may have little effect on R^*_f. Observed effects of etomoxir on R^*_f were consistent with these expectations. Thus, R^*_f in contracting muscle was either substantially decreased or unchanged by etomoxir. In contrast, etomoxir increased R^*_f in all inactive hindlimb muscles, white adipose tissue, and brain.

In conclusion, we have described a novel method for assessing tissue-specific plasma FFA utilization in vivo based on the use of [9,10-^{3}H]-(R)-2-bromopalmitate. Our initial investigation indicates the potential of the method as a useful tool for in vivo studies of plasma FFA transport and utilization, particularly in adipose tissues and skeletal muscles. Indices of plasma FFA utilization obtained for liver and heart should be interpreted more cautiously because of less effective ^{3}H-labeled metabolite retention in these tissues. Finally, simultaneous use of a native FFA tracer ([^{14}C]palmitate) and [9,10-^{3}H]-(R)-2-bromopalmitate increases the power of the method by providing tissue-specific information on the metabolic fate (oxidative versus non-oxidative disposal) of metabolically sequestered FFAs.

APPENDIX

Determination of plasma ^{3}H-R-BrP and ^{14}C-P

Small corrections were made for incomplete partitioning of ^{3}H-R-BrP and ^{14}C-P into the alcohol phase of the extraction system in the following way. Assuming all lipid-extractable radioactivity was associated with either FFA (F, either ^{3}H-R-BrP or ^{14}C-P) or EFA (T), then the relationship to measured radioactivity levels in the alcohol (A), and hexane fractions (H) is given by the two simultaneous equations: (i) $A = (1 - c_{TH})\ T + c_{FA}F$ and (ii) $H = c_{TH}\ T + (1 - c_{FA})\ F$; where c_{TH} and c_{FA} are the partition coefficients for EFA into hexane, and free fatty acid into alcohol, respectively. Equations were solved for F and T. Values for the coefficients were obtained using pure fatty acid (infusate ^{3}H-R-BrP and ^{14}C-P) and triglyceride ([carboxyl-^{14}C]triolein, NEN, Boston, MA) standards. The partition coefficients were measured for each extraction run but were very reproducible ($c_{TH} \sim 0.98$, $c_{FA} \sim 0.90$).

Theory and mathematical analysis: calculation of R^*_f

It is assumed that ^{3}H-R-BrP undergoes the same initial transport steps and activation reaction as the native FFAs. Beyond the activation step, mediated by the enzyme ACS, the metabolic handling of the analog diverges from the native compounds. We assume that radioactive atoms derived from ^{3}H-R-BrP are effectively trapped in the cells. Given the additional assumption of system stationarity which, inter alia, presumes that the system is unperturbed by the presence of tracer quantities of 2-bromopalmitate, then the following expression for tissue-specific utilization rate of FFA (R_f) can be written (see ref. 31 for a treatment of the general mathematical problem):

$$R_f = \frac{C_P m_B(\infty)}{LC^* \int_0^\infty c_B(t)dt}$$

where C_P is the arterial plasma FFA concentration, m_B is the tissue concentration of radioactivity associated with metabolized products of ^{3}H-R-BrP, c_B is the arterial plasma concentration of ^{3}H-R-BrP as a function of time (t) after a short infusion of ^{3}H-R-BrP. LC^* represents the ratio of the probability that a molecule of arterial ^{3}H-R-BrP will undergo activation to ^{3}H-R-BrP-CoA, to the probability that a molecule of arterial palmitate will undergo activation to palmitoyl-CoA. This parameter is equivalent to the so-called "lumped constant" defined for 2-deoxyglucose (9). LC^* is a function of several individual mass transfer coefficients and would equal 1 if ^{3}H-R-BrP kinetics were identical to the native compound, up to and including the activation step.

For an experiment conducted over a finite length of time, the following approximation

$$R_f \approx \frac{C_P m_B(T)}{LC^* \int_0^T c_B(t)dt}$$

Downloaded from www.jlr.org by guest, on June 14, 2012

would be valid for experiments of sufficiently long duration (T) such that $c_B(T) \approx 0$ and where the tissue concentration of non-metabolized ^{3}H-R-BrP $<<$ m_B. For practical application, we define an index of plasma FFA utilization (R^*_f) in terms of measurable ^{3}H-R-BrP kinetic parameters as

$$R^*_f = \frac{C_P m_B(T)}{\int_0^T c_B(t)dt}$$

noting that for sufficiently long T, $R^*_f \approx LC^* R_f$.

Plasma ^{3}H-R-BrP and ^{14}C-P activity data: function fits and calculation of integrals

Regarding the method of tracer delivery, very rapid plasma disappearance kinetics of ^{3}H-R-BrP and ^{14}C-P led us to adopt a short infusion protocol as an alternative to the bolus injection approach. Plasma ^{3}H-R-BrP data were fitted (using non-linear regression analysis) to the four parameter function

$$\mathcal{C}_B(t) = \frac{1}{T_{in}} \sum_{i=1}^{2} \left\{ \frac{A_i}{\lambda_i} [(1 - e^{-\lambda_i t}) - S_{T_{in}}(1 - e^{-\lambda_i (t - T_{in})})] \right\}$$

where T_{in} is the tracer infusion time, $S_{T_{in}}$ is a step function ($S_{T_{in}} = 0$ at $t < T_{in}$; $S_{T_{in}} = 1$ at $t \geq T_{in}$). A completely analogous expression was used for fitting the plasma ^{14}C-P data. Integrals of the plasma activity functions, required for evaluating the whole body and tissue-specific turnover parameters as well as initial distribution volumes for ^{3}H-R-BrP and ^{14}C-P, were calculated analytically using the parameters obtained from the "best" fits. Goodness-of-fit was quantitatively assessed using a chi-square test (38) comparing residuals with estimates of experimental error based on the variation of group data at individual time points. The criteria for an acceptable fit was $P > 0.05$.

Estimation of the lumped constant *LC**

For estimation of LC^* consider an experiment where ^{14}C-P and ^{3}H-R-BrP tracers are simultaneously introduced into plasma as a short infusion. It is assumed that after the ACS-mediated activation step, palmitoyl-CoA is directed into either *i*) oxidation, in which case the radiolabeled products of ^{14}C-P, notably $^{14}CO_2$, are very rapidly cleared from the cells and do not contribute to tissue activity at the time of tissue sampling, or *ii*) storage (e.g., esterification), where all radiolabeled products of ^{14}C-P are effectively trapped in the tissue. Thus, total FFA utilization rate can be written as the sum of the storage (R_{fs}) and oxidative pathways (R_{fo}), i.e.,

$$R_f = R_{fs} + R_{fo}$$

and an estimate of the flux component of fatty acid utilization directed into storage (R_{fs}') can be obtained from the expression

$$R_{fs}' = \frac{C_P m_P(T)}{\int_0^T c_P(t)dt}$$

where m_P is the tissue concentration of radioactivity associated with metabolized products of ^{14}C-P, c_P is the arterial plasma concentration of ^{14}C-P as a function of time (t), and T is the time of tissue sampling. Under conditions where $R_{fo} << R_f$ (e.g., during β-oxidation blockade) this approximation should be improved. As under these conditions $R^*_f \approx LC^* R_{fs}$ an estimate of LC^* can be obtained using the expression

$$LC^* \approx R^*_f / R_{fs}'$$

Analysis of tissue ^{3}H retention data

To assess the assumption that metabolites of ^{3}H-R-BrP are effectively trapped, tissue ^{3}H activity 16 min after tracer administration (standard duration control group) was compared to tissue activity 60 min after tracer administration (extended duration control group). Retention over the standard 16 min experiment was estimated in the following way. Assuming *i*) that by 16 min all tissue activity was associated with metabolized products of ^{3}H-R-BrP and that this material existed in a single kinetically homogeneous pool, *ii*) by 16 min entry of newly formed material into this pool had practically ceased, and *iii*) efflux from the pool was irreversible and directly into plasma. If it were possible to pulse label the metabolite pool then we would have

$$m_B(t) = m_B(0)e^{-t\lambda}$$

where m_B (0) is the tissue content of ^{3}H activity associated with metabolized products of ^{3}H-R-BrP at $t = 0$, λ is the first order rate constant for loss of tissue activity, which was estimated from the tissues collected at t = 16 and t = 60 min. Retention of ^{3}H activity over the standard 16-min experiment was then calculated using the λ estimates.

Manuscript received 14 December 1998 and in revised form 25 February 1999.

REFERENCES

1. Ferrannini, E. 1988. The theoretical bases of indirect calorimetry: a review. *Metab. Clin. Exp.* **37:** 287–301.
2. Miles, J. M., M. G. Ellman, K. L. McClean, and M. D. Jensen. 1987. Validation of a new method for determination of free fatty acid turnover. *Am. J. Physiol.* **252:** E431–E438.
3. Wisneski, J. A., E. W. Gertz, R. A. Neese, and M. Mayr. 1987. Myocardial metabolism of free fatty acids. Studies with ^{14}C-labeled substrates in humans. *J. Clin. Invest.* **79:** 359–366.
4. Natali, A., G. Buzzigoli, S. Taddei, D. Santoro, M. Cerri, R. Pedrinelli, and E. Ferrannini. 1990. Effects of insulin on hemodynamics and metabolism in human forearm. *Diabetes.* **39:** 490–500.
5. Martin, G., K. Schoonjans, A. M. Lefebvre, B. Staels, and J. Auwerx. 1997. Coordinate regulation of the expression of the fatty acid transport protein and acyl-CoA synthetase genes by PPARalpha and PPARgamma activators. *J. Biol. Chem.* **272:** 28210–28217.
6. Niot, I., H. Poirier, and P. Besnard. 1997. Regulation of gene expression by fatty acids: special reference to fatty acid-binding protein (FABP). *Biochimie.* **79:** 129–133.
7. Turcotte, L. P., A. K. Srivastava, and J. L. Chiasson. 1997. Fasting increases plasma membrane fatty acid-binding protein (FABP(PM)) in red skeletal muscle. *Mol. Cell. Biochem.* **166:** 153–158.

Downloaded from www.jlr.org by guest, on June 14, 2012

8. Glatz, J. F., F. A. van Nieuwenhoven, J. J. Luiken, F. G. Schaap, and G. J. van der Vusse. 1997. Role of membrane-associated and cytoplasmic fatty acid-binding proteins in cellular fatty acid metabolism. *Prostaglandins Leukot. Essent. Fatty Acids.* **57:** 373–378.
9. Sokoloff, L., M. Reivich, C. Kennedy, M. H. Des Rosiers, C. S. Patlak, K. D. Pettigrew, O. Sakurada, and M. Shinohara. 1977. The [^{14}C]deoxyglucose method for the measurement of local cerebral glucose utilization: theory, procedure, and normal values in the conscious and anesthetized albino rat. *J. Neurochem.* **28:** 897–916.
10. Livni, E., D. R. Elmaleh, M. M. Barlai-Kovach, M. M. Goodman, F. F. Knapp, Jr., and H. W. Strauss. 1985. Radioiodinated beta-methyl phenyl fatty acids as potential tracers for myocardial imaging and metabolism. *Eur. Heart J.* **6:** 85–89.
11. Miller, D. D., J. B. Gill, A. J. Fischman, R. J. Callahan, D. R. Elmaleh, C. A. Boucher, and H. W. Strauss. 1986. New radionuclides for cardiac imaging. *Prog. Cardiovasc. Dis.* **28:** 419–434.
12. Fink, G. D., J. A. Montgomery, F. David, M. Garneau, E. Livni, D. Elmaleh, H. W. Strauss, and H. Brunengraber. 1990. Metabolism of beta-methyl-heptadecanoic acid in the perfused rat heart and liver. *J. Nucl. Med.* **31:** 1823–1830.
13. Kawamoto, M., N. Tamaki, Y. Yonekura, Y. Magata, E. Tadamura, R. Nohara, A. Matsumori, S. Sasayama, and J. Konishi. 1994. Significance of myocardial uptake of iodine 123-labeled beta-methyl iodophenyl pentadecanoic acid: comparison with kinetics of carbon 11-labeled palmitate in positron emission tomography. *J. Nucl. Cardiol.* **1:** 522–528.
14. Schulz, G., J. von Dahl, H. J. Kaiser, K. C. Koch, O. Sabri, L. Banneitz, U. Cremerius, and U. Buell. 1996. Imaging of beta-oxidation by static PET with 14(R,S)-[18F]-fluoro-6-thiaheptadecanoic acid (FTHA) in patients with advanced coronary heart disease: a comparison with 18FDG-PET and 99Tcm-MIBI SPET. *Nucl. Med. Commun.* **17:** 1057–1064.
15. Peeters, R. A., M. A. in't Groen, M. P. de Moel, H. T. van Moerkerk, and J. H. Veerkamp. 1989. The binding affinity of fatty acid-binding proteins from human, pig and rat liver for different fluorescent fatty acids and other ligands. *Int. J. Biochem.* **21:** 407–418.
16. Buechler, K. F., and J. M. Lowenstein. 1990. The involvement of carnitine intermediates in peroxisomal fatty acid oxidation: a study with 2-bromofatty acids. *Arch. Biochem. Biophys.* **281:** 233–238.
17. Chase, J. F., and P. K. Tubbs. 1972. Specific inhibition of mitochondrial fatty acid oxidation by 2-bromopalmitate and its coenzyme A and carnitine esters. *Biochem. J.* **129:** 55–65.
18. McGarry, J. D., A. Sen, V. Esser, K. F. Woeltje, B. Weis, and D. W. Foster. 1991. New insights into the mitochondrial carnitine palmitoyltransferase enzyme system. *Biochimie.* **73:** 77–84.
19. Spector, A. A. 1986. Biochemistry and Biology of Plasma Lipoproteins. Marcel Dekker, New York. 247–279.
20. Epps, D. E., T. J. Raub, and F. J. Kezdy. 1995. A general, wide-range spectrofluorometric method for measuring the site-specific affinities of drugs toward human serum albumin. *Anal. Biochem.* **227:** 342–350.
21. Kinkaid, A. R., and D. C. Wilton. 1993. A continuous fluorescence displacement assay for phospholipase A2 using albumin and medium chain phospholipid substrates. *Anal. Biochem.* **212:** 65–70.
22. Tanaka, T., K. Hosaka, and S. Numa. 1981. Long-chain acyl-CoA synthetase from rat liver. *Methods Enzymol.* **71:** 334–341.
23. Harwood, H. J. 1962. Reactions of the hydrocarbon chain of fatty acids. *Chem. Rev.* **62:** 102–103.
24. Forsberg, G., S. Andersson, R. L. Simonsson, and G. I. Hansson. 1998. Analytical and semi-preparative high performance liquid chromatographic separation of the enantiomers of 2-bromopalmitic acid in plasma. 22nd International Symposium on High Performance Liquid Phase Separations and Related Techniques 1998.
25. Kirchner, G., M. P. Scollar, and A. M. Klibanov. 1985. Resolution of racemic mixtures via lipase catalysis in organic solvents. *J. Am. Chem. Soc.* **107:** 7072–7076.
26. Hernanz, D., F. Camps, A. Guerro, and A. Delgado. 1985. Synthesis and configurational assignment of (R) and (S)-2-bromohexadecanoic acids. *Tetrahedron Asymmetry.* **6:** 2291–2298.
27. Hagenfeldt, L. 1966. A gas chromatographic method for the determination of individual free fatty acids in plasma. *Clin. Chim. Acta.* **13:** 266–268.
28. Maatman, R. G., H. T. van Moerkerk, I. M. Nooren, E. J. van Zoelen, and J. H. Veerkamp. 1994. Expression of human liver fatty acid-binding protein in *Escherichia coli* and comparative analysis of its binding characteristics with muscle fatty acid-binding protein. *Biochim. Biophys. Acta.* **1214:** 1–10.
29. Oakes, N. D., S. Camilleri, S. M. Furler, D. J. Chisholm, and E. W. Kraegen. 1997. The insulin sensitizer, BRL 49653, reduces systemic fatty acid supply and utilization and tissue lipid availability in the rat. *Metab. Clin. Exp.* **46:** 935–942.
30. Sokal, R. R., and F. J. Rohlf. 1969. Biometry. W. H. Freeman, San Francisco.
31. Patlak, C. S. 1981. Derivation of equations for the steady-state reaction velocity of a substance based on the use of a second substance. *J. Cereb. Blood Flow Metab.* **1:** 129–131.
32. Weaner, L. E., and D. C. Hoerr. 1987. A high-performance liquid chromatographic method for the enantiomeric analysis of the enzymatically synthesized coenzyme A ester of 2-tetradecylglycidic acid. *Anal. Biochem.* **160:** 316–322.
33. Chen, C. S., W. R. Shieh, P. H. Lu, S. Harriman, and C. Y. Chen. 1991. Metabolic stereoisomeric inversion of ibuprofen in mammals. *Biochim. Biophys. Acta.* **1078:** 411–417.
34. Declercq, P. E., J. R. Falck, M. Kuwajima, H. Tyminski, D. W. Foster, and J. D. McGarry. 1987. Characterization of the mitochondrial carnitine palmitoyltransferase enzyme system. I. Use of inhibitors. *J. Biol. Chem.* **262:** 9812–9821.
35. Sidossis, L. S., A. R. Coggan, A. Gastaldelli, and R. R. Wolfe. 1995. Pathway of free fatty acid oxidation in human subjects. Implications for tracer studies. *J. Clin. Invest.* **95:** 278–284.
36. Ng, C. K., J. E. Holden, T. R. DeGrado, D. M. Raffel, M. L. Kornguth, and S. J. Gatley. 1991. Sensitivity of myocardial fluorodeoxyglucose lumped constant to glucose and insulin. *Am. J. Physiol.* **260:** H593–603.
37. Skorin, C., C. Necochea, V. Johow, U. Soto, A. M. Grau, J. Bremer, and F. Leighton. 1992. Peroxisomal fatty acid oxidation and inhibitors of the mitochondrial carnitine palmitoyltransferase I in isolated rat hepatocytes. *Biochem. J.* **281:** 561–567.
38. Press, W. H., B. P. Flannery, S. A. Teukolsky, and W. T. Vetterling. 1986. Numerical Recipes. Cambridge University Press, Cambridge, UK. 502–503.

Downloaded from www.jlr.org by guest, on June 14, 2012